J Mater Sci (2020) 55:5730–5740

Ceramics

Phase transition temperature and negative thermal expansion of Sc-substituted $In_2(MoO_4)_3$ ceramics

Zhiping Zhang[1], Yuenan Wang[2], Weikang Sun[2], Xiuyun Zhang[2], Hongfei Liu[2,*], Xiaobing Chen[2], and Xianghua Zeng[2]

[1] Guangling College, Yangzhou University, Yangzhou 225009, People's Republic of China
[2] School of Physical Science and Technology, Yangzhou University, Yangzhou 225002, People's Republic of China

Received: 28 October 2019
Accepted: 10 February 2020
Published online: 16 February 2020

ABSTRACT

A series of Sc-substituted $In_2Mo_3O_{12}$ ceramics were synthesized by the chemical co-precipitation method. The results reveal that In^{3+} can be substituted by Sc^{3+} and form a single phase with high purity for all $In_{2-x}Sc_xMo_3O_{12}$ (x = 0, 0.3, 0.6, 0.9, 1.2 and 1.5) samples. The crystal structure of $In_{2-x}Sc_xMo_3O_{12}$ changes from monoclinic to orthorhombic symmetry with increasing Sc^{3+}-content, confirmed by X-ray diffraction and Raman spectroscopy (Raman). With increasing concentration of A-site Sc^{3+} cations, the microstructure of $In_{2-x}Sc_xMo_3O_{12}$ becomes denser and the shape and size distribution of grains is more regular and uniform. The monoclinic-to-orthorhombic phase transition temperature of $In_2Mo_3O_{12}$ is successfully decreased from 343 °C to room temperature via the substitution of In^{3+} by Sc^{3+}. When x = 1.5, the occurrence of the monoclinic-to-orthorhombic phase transition for $In_{0.5}Sc_{1.5}Mo_3O_{12}$ solid solution is at around 7 °C. It has an average linear coefficient of thermal expansion of -5.08×10^{-6} °C^{-1} in 25–600 °C. The phase transition results obtained by theoretical calculation using the framework of spin-polarized DFT accord well with the experimental evidences.

Introduction

In general, most of the materials expand as the temperature rises, but some materials exhibit anomalous thermal expansion, which is called negative thermal expansion (NTE). Such materials contract as they are heated up and expand as they are cooled down. They have attracted extensive attention due to their special physical properties, which have potential applications in optical and microelectronic devices. Previous studies in $A_2Mo_3O_{12}$ (A = trivalent main group metal or transition metal and M = W, Mo) reveal that many of them exhibit NTE [1–6]. When the A-site is occupied by Y^{3+}, Ho^{3+}, Tm^{3+}, Er^{3+}, Yb^{3+} and Lu^{3+}, these $A_2Mo_3O_{12}$ materials form hydrated polymorphs that display positive thermal expansion (PTE) at room temperature because they are highly hygroscopic in the air. The water that is incorporated into the crystal structure hinders the transverse vibrations of the A–O–M linkages, ultimately leading to the complete loss

Address correspondence to E-mail: liuhf@yzu.edu.cn

https://doi.org/10.1007/s10853-020-04441-9

of NTE. Only when the absorbed water is volatilized by heating can these $A_2Mo_3O_{12}$ materials exhibit strong NTE. This reversible hygroscopicity severely restricts any practical applications of such materials [7–16]. No hygroscopicity has been observed in $A_2Mo_3O_{12}$ (A = Sc, Al, In, Cr, Fe) molybdates as well as $Sc_2W_3O_{12}$ tungstate [3, 4, 17]. However, in the above cases, $A_2Mo_3O_{12}$ materials exhibit PTE with a monoclinic structure at low temperature, and NTE behavior can only be observed in an orthorhombic structure at high temperature upon undergoing a phase transition from monoclinic to orthorhombic.

$In_2Mo_3O_{12}$ exhibits very strong NTE in its orthorhombic phase, making it a promising candidate for tuning coefficients of thermal expansion (CTE) in composites. $In_2Mo_3O_{12}$ undergoes the monoclinic-to-orthorhombic phase transition at 340 °C [4]. Its solid solution suffers, however, from destruction by thermal cracking caused by the occurrence of the phase transition throughout the working temperature.

The dependence of the phase transition temperature for $A_2(MO_4)_3$ on the electronegativity of the A-site cation has been reported. For example, the electronegativity of Sc^{3+} is the lowest among the non-hygroscopic A-site cations in the $A_2M_3O_{12}$ series. Accordingly, the phase transition temperatures of $Sc_2Mo_3O_{12}$ and $Sc_2W_3O_{12}$ are also lowest, at about − 95 °C and − 263 °C (or lower), respectively. In an attempt to stabilize the orthorhombic phase at room temperature, the A-site cation in $In_2Mo_3O_{12}$ is partially substituted by low-electronegativity Sc^{3+} to suppress the undesirable phase transition. In previous work by our group, a new series of $In_{2-x}Sc_xMo_3O_{12}$ solid solutions synthesized by the solid-state method suffer from high energy consumption, incomplete reaction and low density [18]. It is well known that the chemical co-precipitation method can overcome these disadvantages of the solid-state method.

This study is devoted to the preparation of a series of $In_{2-x}Sc_xMo_3O_{12}$ solid solutions with high density and the stabilization of the orthorhombic phase of $In_2Mo_3O_{12}$ at room temperature or lower by tuning the content of Sc^{3+}-substitution. In this paper, $In_{2-x}Sc_xMo_3O_{12}$ solid solutions are synthesized by the chemical co-precipitation method. The effects of Sc^{3+}-substitution on its crystal structure, phase transition, micromorphology, density as well as negative thermal expansion of $In_2Mo_3O_{12}$ have been studied. From the combined experimental results, the correlation between Sc^{3+}-substitution and NTE as well as the phase transition temperature of $In_2Mo_3O_{12}$ can be well established. In this work, to investigate the phase transfer process of $In_{2-x}Sc_xMo_3O_{12}$, the total energies of both monoclinic and orthorhombic phase $In_{2-x}Sc_xMo_3O_{12}$ with various doping atomic ratios of Sc^{3+} are also calculated using spin-polarized density functional theory.

Experimental details

The series of $In_{2-x}Sc_xMo_3O_{12}$ solid solutions were synthesized by the chemical co-precipitation method using commercially available $In(NO_3)_3{\cdot}xH_2O$, $Sc(NO_3)_3{\cdot}6H_2O$ and $(NH_4)_6Mo_7O_{24}{\cdot}4H_2O$ as raw materials. The starting reactants were weighed in stoichiometric amounts corresponding to In^{3+}:Sc^{3+}:Mo^{6+} molar ratios of 2:0:3, 1.7:0.3:3, 1.4:0.6:3, 1.1:0.9:3, 0.8:1.2:3 and 0.5:1.5:3 and dissolved in deionized water. The three solutions were mixed in a total volume of 25 ml of deionized water while stirring at 80 °C. The pH value of the solution was kept around 10, which was controlled by dripping in ammonia as needed. The corresponding slurries were stirred for 2 h and then dried at 90 °C. The obtained powder was pre-sintered at 500 °C, followed by cold isostatic pressing into pellets (7 mm in diameter), and finally sintered at 760 °C for 6 h in air.

The structural characterization was determined by the X-ray diffraction (XRD) technique, using a Shimadzu XRD-7000 with CuKα radiation. Data were collected with a scanning speed of 5°/min. Raman spectra were collected (Thermo Fisher, DXRxi) in the scanning range of 100–1200 cm^{-1} with a power of 0.2 mW using a laser with a wavelength of 532 nm. Elemental mapping was done by energy-dispersive X-ray spectroscopy (EDX) on a high-resolution transmission electron microscopy (HRTEM, FEI Tecnai F30 S-TWIN). X-ray photoelectron spectroscopy (XPS, Thermo Scientific, ESCALAB 250Xi) was used to study the valence state of all elements. The cross-sectional microstructure was characterized by scanning electron microscopy (SEM, TESCAN VEEGA3). Dilatometric studies were performed on pellets at a heating rate of 5 °C/min from room temperature to 600 °C using thermal mechanical analysis (TMA/SS, Seiko 6300). Differential scanning calorimetry (DSC) measurements were carried out using PerkinElmer

DSC-8500, with the heating rate of 5 °C/min from room temperature to 350 °C.

Results and discussion

Crystal structure analysis

The crystal structure of the samples was determined by X-ray diffraction. The XRD patterns of as-synthesized $In_{2-x}Sc_xMo_3O_{12}(0 \le x \le 1.5)$ heat-treated at different temperatures are shown in Fig. 1. As shown in Fig. 1a, the samples are crystallized during pre-sintering at 500 °C. The crystallization temperature is relatively lower compared to that of solid-state reaction method [18], which means that the chemical co-precipitation synthesis can cause good sinterability of samples. To improve the crystallinity and density, the sintering temperature was further increased to 760 °C and the corresponding XRD patterns are shown in Fig. 1b. All the diffraction peaks become stronger and sharper with no variation in positions, revealing that the crystallinity of the samples is improved with increased sintering temperature. For comparison, the reference pattern for monoclinic $In_2(MoO_4)_3$ is also displayed. All $In_{2-x}Sc_x(MoO_4)_3$ ceramics with Sc^{3+}-content (x) ranging from 0.3 to 1.2 appear to be a well-crystallized single phase with monoclinic $In_2(MoO_4)_3$-type structure, and no impurity phases are detected. As the Sc^{3+}-content (x) is increased to 1.5, $In_{0.5}Sc_{1.5}Mo_3O_{12}$ crystallizes in an orthorhombic $Sc_2(MoO_4)_3$-type structure (space group *Pbcn*, JCPDS card No.21-1329), as marked by the disappearance of the diffraction peaks at 2θ = 25°–27.5° (Fig. 2).

As the small differences between the monoclinic and orthorhombic crystal structures of $In_{2-x}Sc_xMo_3O_{12}$ can make them difficult to distinguish through XRD, Raman analysis was carried out to further characterize the different phases, and the results are depicted in Fig. 3. For x = 0, the recorded Raman spectrum of $In_2Mo_3O_{12}$ agrees well with literature reports [19]. As seen in the spectrum, $In_2Mo_3O_{12}$ presents strong Raman bands with some shoulders in the 970–1030 cm^{-1} and 790–970 cm^{-1} region that can be related to Mo–O symmetric and asymmetric stretching modes, respectively. In addition, the distinct peaks in the 300–400 cm^{-1} range originate from bending modes of the MoO_4 tetrahedra and InO_6 octahedra. Comparison of the spectra as a function of composition reveals that the three characteristic peaks located at 175, 862 and 994 cm^{-1} are gradually

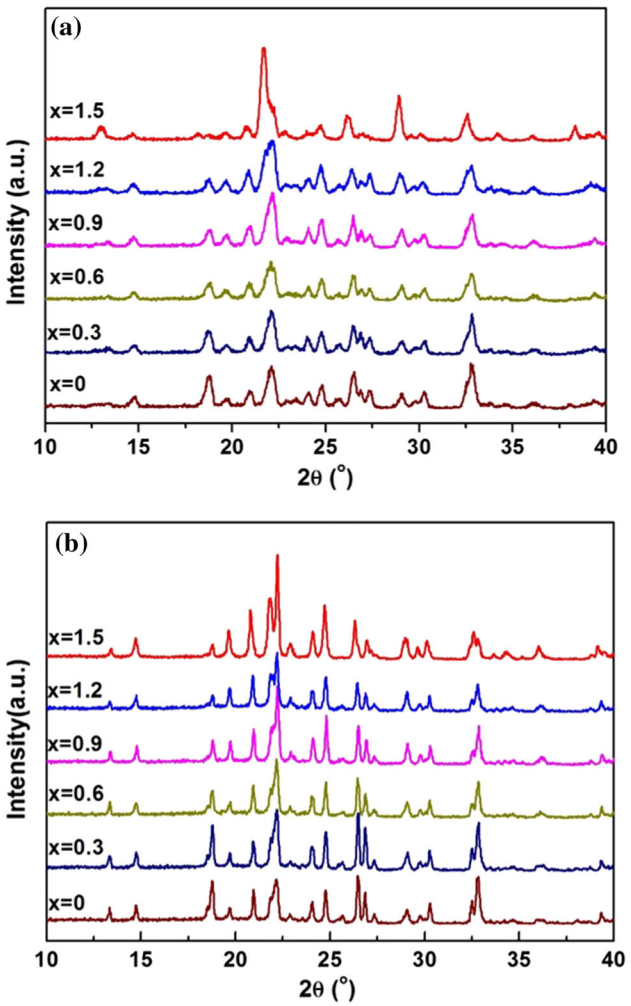

Figure 1 XRD patterns of $In_{2-x}Sc_xMo_3O_{12}$ (x = 0, 0.3, 0.6, 0.9, 1.2 and 1.5) sintered for 6 h at **a** 500 °C and **b** 760 °C.

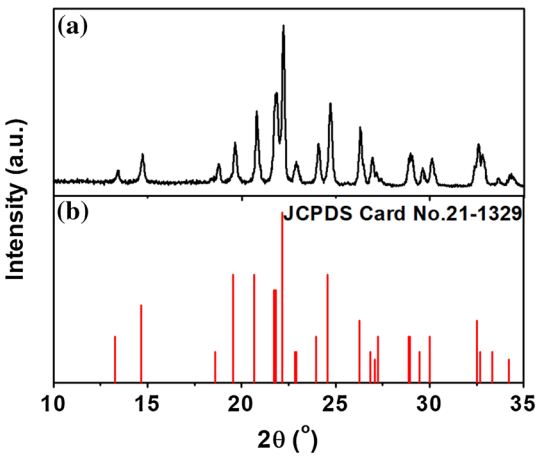

Figure 2 a X-ray diffraction pattern of $In_{0.5}Sc_{1.5}Mo_3O_{12}$ and b $Sc_2Mo_3O_{12}$ reference pattern.

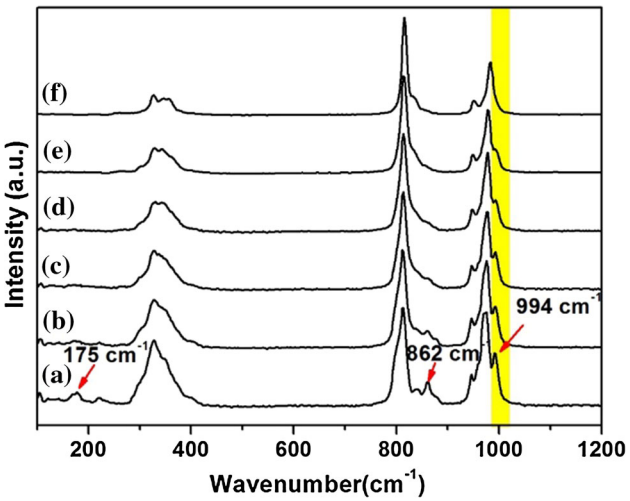

Figure 3 The Raman spectra of $In_{2-x}Sc_xMo_3O_{12}$ solid solutions a $In_2Mo_3O_{12}$, b $In_{1.7}Sc_{0.3}Mo_3O_{12}$, c $In_{1.4}Sc_{0.6}Mo_3O_{12}$, d $In_{1.1}Sc_{0.9}Mo_3O_{12}$, e $In_{0.8}Sc_{1.2}Mo_3O_{12}$ and f $In_{0.5}Sc_{1.5}Mo_3O_{12}$.

weakened with increasing Sc^{3+}-content (x) and disappear completely around $x = 1.5$ (Fig. 3f). The Raman spectrum of $In_{0.5}Sc_{1.5}Mo_3O_{12}$ corresponds to the typical spectrum of orthorhombic $Sc_2Mo_3O_{12}$ in exact accordance with literature data [19]. This observation suggests that the crystal structure of $In_{0.5}Sc_{1.5}Mo_3O_{12}$ has changed from monoclinic to orthorhombic symmetry at room temperature, in good agreement with the above XRD analysis.

To further confirm the successful synthesis of single-phased samples, EDX, STEM and XPS were performed on the $In_{0.5}Sc_{1.5}Mo_3O_{12}$ solid solution. In, Mo, O, Sc and C used for calibration are detected in $In_{0.5}Sc_{1.5}Mo_3O_{12}$ (Fig. 4a), and the corresponding high-resolution XPS spectra of the In 3*d* and Sc 2*p* are shown in Fig. 4b, c, respectively. Two peaks at the binding energy of 445 eV and 453 eV are assigned to In $3d_{5/2}$ and In $3d_{3/2}$ of trivalent indium. In addition, the two peaks with binding energies of 403 eV and 407 eV are attributed to Sc $2p_{3/2}$ and Sc $2p_{1/2}$, indicating the existence of trivalent scandium. The homogeneity of the elemental composition of $In_{0.5}Sc_{1.5}Mo_3O_{12}$ was further demonstrated through EDX analysis, as shown in Fig. 4d. No elements other than In, Mo, O, Sc and Cu are detected. The strong Cu signal originates from the copper net used to mount the sample. Moreover, as shown in Fig. 4e–i, the STEM image and elemental maps of a selected particle for $In_{0.5}Sc_{1.5}Mo_3O_{12}$ powder demonstrate that the four elements are uniformly distributed throughout the investigated region. Based on the above analysis, these results clearly confirm that In^{3+} is substituted by Sc^{3+} in $In_2Mo_3O_{12}$ to form a single phase with high purity.

To better understand the crystal structure of $In_{2-x}Sc_xMo_3O_{12}$, the ball-and-stick model presentations are given in Fig. 5; $In_2Mo_3O_{12}$ takes on a monoclinic structure (see Fig. 5a), while $In_{0.5}Sc_{1.5}Mo_3O_{12}$ adopts an orthorhombic structure at room temperature (see Fig. 5b), and the frameworks of both are composed of a network of InO_6 (ScO_6) octahedra and MoO_4 tetrahedra. Mo^{6+} occupies the center of MoO_4 tetrahedra. In^{3+} occupies the center of InO_6 octahedra. With the increase in Sc^{3+}-substitution content, Sc^{3+} gradually replaces In^{3+} and occupies the A-sites in the center of InO_6 octahedra, which is shown in Fig. 5c. Sc^{3+}-substitution leads to the change in crystal structure from monoclinic to orthorhombic symmetry.

Microstructure analysis

To reveal the relationship between the microstructure and substituted Sc^{3+}-content (x), the typical cross-sectional morphologies of $In_{2-x}Sc_xMo_3O_{12}$ solid solutions are shown in Fig. 6. It is observed that all samples exhibit a dense microstructure without significant pores in contrast to the solid solutions synthesized by the solid-state method [18], indicating a great improvement in the density of solid solutions. In the case of pure $In_2Mo_3O_{12}$, the average size of particles varies from 2 to 10 μm and the shapes of particles are not regular (Fig. 6a). Moreover, SEM micrographs clearly reveal the dependence of grain size, as well as the homogeneity of grain sizes, on Sc^{3+}-content (x): The average grain size is gradually reduced and the uniformity of the grain size is improved with increasing Sc^{3+}-content. For $x = 1.2$, the average grain size is reduced to 2–3 μm, and the microstructure morphology of $In_{0.8}Sc_{1.2}Mo_3O_{12}$ solid solution is clearly more regular with spherical shapes (Fig. 6e). For composition $x = 1.5$, $In_{0.5}Sc_{1.5}Mo_3O_{12}$ solid solution displays a uniform grain size distribution and the particle size is further reduced to 1 μm, as shown in Fig. 6f.

To attempt to investigate the effect of substituted Sc^{3+}-content (x) on the relative densities of $In_{2-x}Sc_xMo_3O_{12}$ solid solutions, Archimedes' method was performed on all samples. It can be found that the relative densities for $In_{2-x}Sc_xMo_3O_{12}$ slightly increase with the increase in Sc^{3+}-content (x), which is

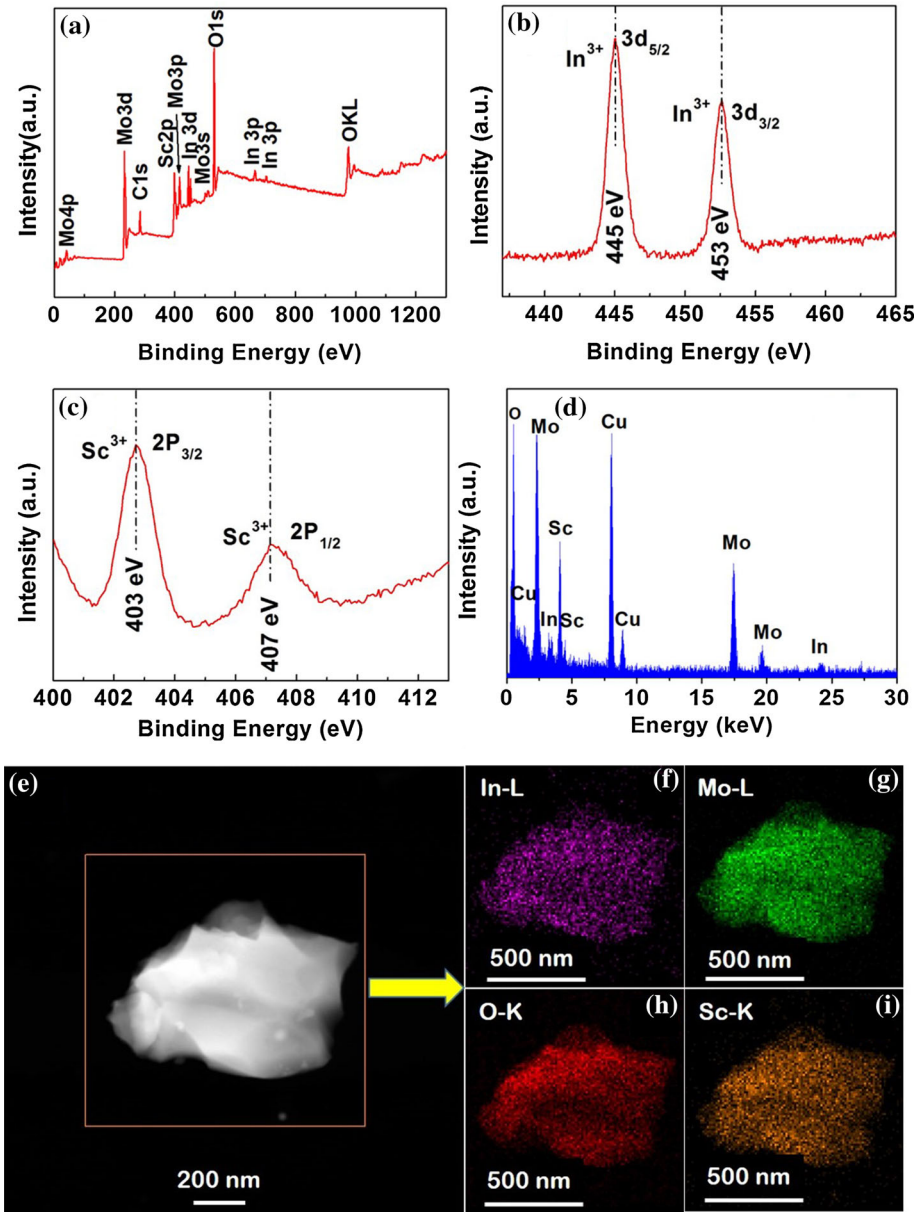

Figure 4 XPS spectra of **a** $In_{0.5}Sc_{1.5}Mo_3O_{12}$, **b** In 3d peaks, **c** Sc 2p peaks, **d** EDX spectrum and **e** STEM micrograph of $In_{0.5}Sc_{1.5}Mo_3O_{12}$ powder and **f** In, **g** Mo, **h** O, **i** Sc elemental mapping images.

consistent with the SEM observations. Furthermore, the average relative densities of $In_{2-x}Sc_xMo_3O_{12}$ solid solutions were found to be about 93% (Fig. 7). Obviously, compared with samples prepared by the solid-state method [18], it can be generalized that the microstructure of $In_{2-x}Sc_xMo_3O_{12}$ solid solutions becomes denser without raising the temperature through use of the chemical co-precipitation method.

Phase transition and thermal expansion studies

The thermal expansion behavior of $In_{2-x}Sc_xMo_3O_{12}$ ($0 \le x \le 1.5$) solid solutions is shown in Fig. 8. The abrupt change in the slope of the thermal expansion curves for $In_2Mo_3O_{12}$ can be attributed to the structural phase transition. This means that $In_2Mo_3O_{12}$ maintains the monoclinic structure up to 334 °C, exhibiting positive thermal expansion with a CTE of 10.48×10^{-6} °C^{-1}. The material then undergoes a phase transition in the 334–355 °C temperature range, above which $In_2Mo_3O_{12}$ crystallizes in an

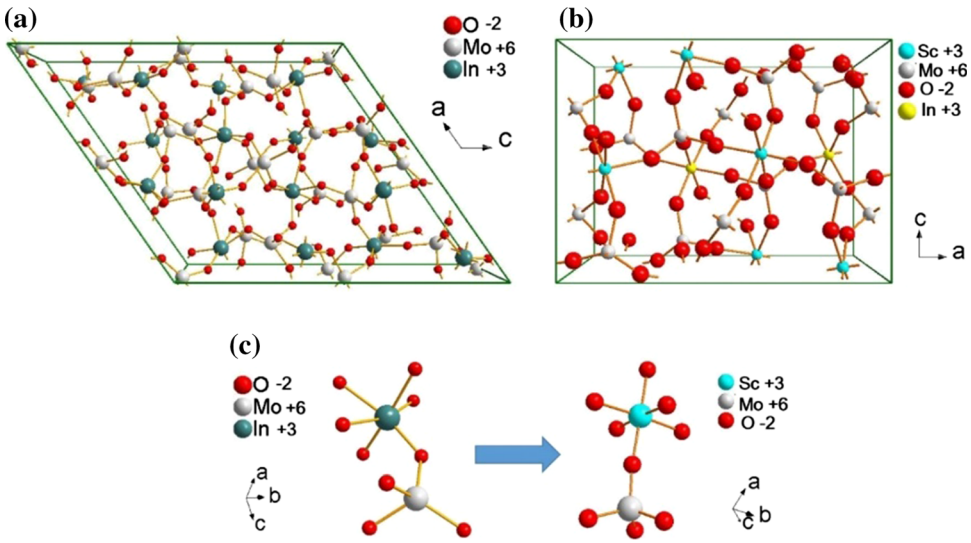

Figure 5 Ball-and-stick model presentations of **a** monoclinic structure for $In_2Mo_3O_{12}$, **b** orthorhombic structure for $In_{0.5}Sc_{1.5}Mo_3O_{12}$, **c** schematic diagram of Sc^{3+} substituting In^{3+} in the crystal structure.

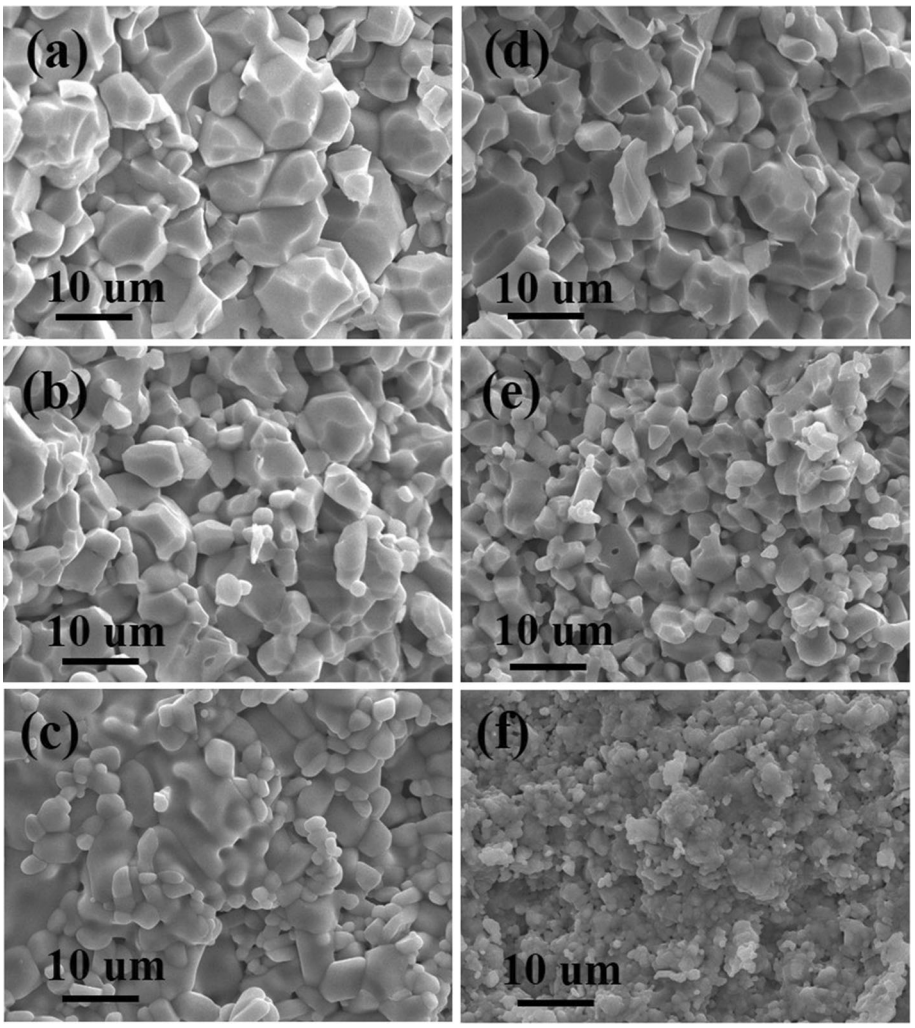

Figure 6 SEM micrographs of $In_{2-x}Sc_xMo_3O_{12}$ solid solutions **a** $In_2Mo_3O_{12}$, **b** $In_{1.7}Sc_{0.3}Mo_3O_{12}$, **c** $In_{1.4}Sc_{0.6}Mo_3O_{12}$, **d** $In_{1.1}Sc_{0.9}Mo_3O_{12}$, **e** $In_{0.8}Sc_{1.2}Mo_3O_{12}$ and **f** $In_{0.5}Sc_{1.5}Mo_3O_{12}$.

orthorhombic structure and exhibits strong NTE with a CTE of -8.36×10^{-6} °C^{-1} from 360 to 600 °C. Similarly, to unsubstituted $In_2Mo_3O_{12}$, all $In_{2-x}Sc_xMo_3O_{12}$ solid solutions follow the same trend, except

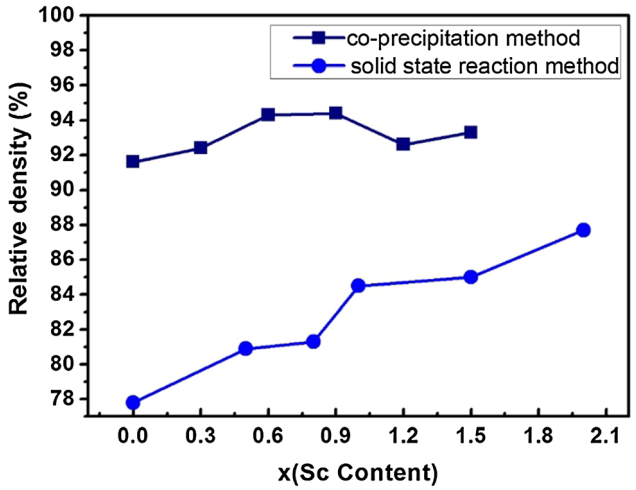

Figure 7 The effect of Sc^{3+}-content on the relative densities of $In_{2-x}Sc_xMo_3O_{12}$ solid solutions prepared by the chemical co-precipitation method and solid-state reaction method, respectively.

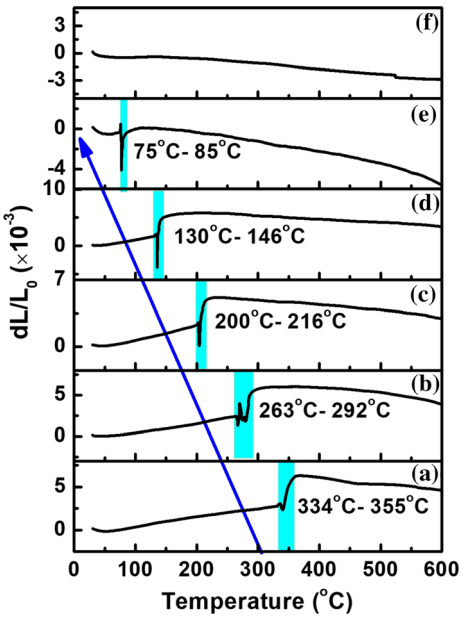

Figure 8 TMA curves of $In_{2-x}Sc_xMo_3O_{12}$ solid solutions a $In_2Mo_3O_{12}$, b $In_{1.7}Sc_{0.3}Mo_3O_{12}$, c $In_{1.4}Sc_{0.6}Mo_3O_{12}$, d $In_{1.1}Sc_{0.9}Mo_3O_{12}$, e $In_{0.8}Sc_{1.2}Mo_3O_{12}$ and f $In_{0.5}Sc_{1.5}Mo_3O_{12}$.

for $In_{0.5}Sc_{1.5}Mo_3O_{12}$. It is worth noting that we have not found any changes in the slope of the curve for $In_{0.5}Sc_{1.5}Mo_3O_{12}$, which shows NTE throughout the testing temperature range. It can be seen that the onset of the phase transition temperature of $In_{2-x}Sc_xMo_3O_{12}$ solid solutions shifts from 334 °C to a temperature of 75 °C as the Sc^{3+}-content increases progressively from $x = 0$ to $x = 1.2$. In addition, A-site substitution with Sc^{3+} not only dramatically decreases the phase transition temperature of $In_2Mo_3O_{12}$, but also gradually narrows the transition range, which is correlated with the electronegativity of the cation. Owning to the lower electronegativity of Sc^{3+} (1.36) compared to that of In^{3+} (1.78), the reduction in the average A-site electronegativity of $(In_{2-x}Sc_x)^{3+}$ as Sc^{3+}-content increases results in increased effective negative charges on the oxygens, and accordingly stronger O–O repulsion, which ultimately results in suppressing the phase transition temperature of $In_{2-x}Sc_xMo_3O_{12}$ to a lower temperature.

The average linear thermal expansion coefficients of the measured $In_{2-x}Sc_xMo_3O_{12}$ solid solutions over the corresponding testing temperature range are summarized in Table 1. $In_{0.5}Sc_{1.5}Mo_3O_{12}$ has an average linear CTE of -5.08×10^{-6} °C^{-1} throughout the testing temperature range.

In order to shed more light on the precise phase transition temperature of $In_{2-x}Sc_xMo_3O_{12}$ solid solutions, differential scanning calorimetry was employed to further characterize the samples, and the results are shown in Fig. 9. The DSC curve of $In_2Mo_3O_{12}$ (Fig. 9a) displays a sharp endothermic peak at 343 °C. We attribute the appearance of this peak to the structural change associated with the monoclinic-to-orthorhombic phase transition. It can be seen that the observed endothermic peak progressively shifts to lower temperatures as the content of Sc^{3+}-substitution increases gradually from $x = 0.3$ to $x = 1.2$. As shown in Fig. 9f, the endothermic peak disappears in the testing temperature range in the case of $x = 1.5$, revealing that the phase transition temperature of $In_{0.5}Sc_{1.5}Mo_3O_{12}$ has been reduced below room temperature. The phase transition temperatures of all $In_{2-x}Sc_xMo_3O_{12}$ solid solutions determined by DSC and TMA are summarized in Table 2 and show good consistency. The correlation between the variation in phase transition temperature and Sc^{3+}-content (x) is established in Fig. 10, which can be used to estimate the phase transition temperature of $In_{2-x}Sc_xMo_3O_{12}$ solid solutions with different contents of Sc^{3+}-substitution. For instance, $Sc_2Mo_3O_{12}$ experiences the phase transition at about − 104.2 °C, which is consistent with the reported data. It could be inferred that the occurrence of the phase transition for $In_{0.5}Sc_{1.5}Mo_3O_{12}$ is at about 7 °C.

Table 1 Average linear thermal expansion coefficient of $In_{2-x}Sc_xMo_3O_{12}$ solid solutions (x = 0, 0.3, 0.6, 0.9, 1.2 and 1.5) over the corresponding testing temperature ranges

Samples	CTE ($\times 10^{-6}$ °C^{-1})	Testing temperature range (°C)	CTE ($\times 10^{-6}$ °C^{-1})	Testing temperature range (°C)
$In_2Mo_3O_{12}$	10.48	52–331	− 8.36	360–600
$In_{1.7}Sc_{0.3}Mo_3O_{12}$	11.49	25–263	− 8.41	327–600
$In_{1.4}Sc_{0.6}Mo_3O_{12}$	14.90	50–202	− 6.32	232–600
$In_{1.1}Sc_{0.9}Mo_3O_{12}$	20.41	25–133	− 5.83	177–600
$In_{0.8}Sc_{1.2}Mo_3O_{12}$	5.93	46–73	− 11.27	116–600
$In_{0.5}Sc_{1.5}Mo_3O_{12}$	–	–	− 5.08	25–600

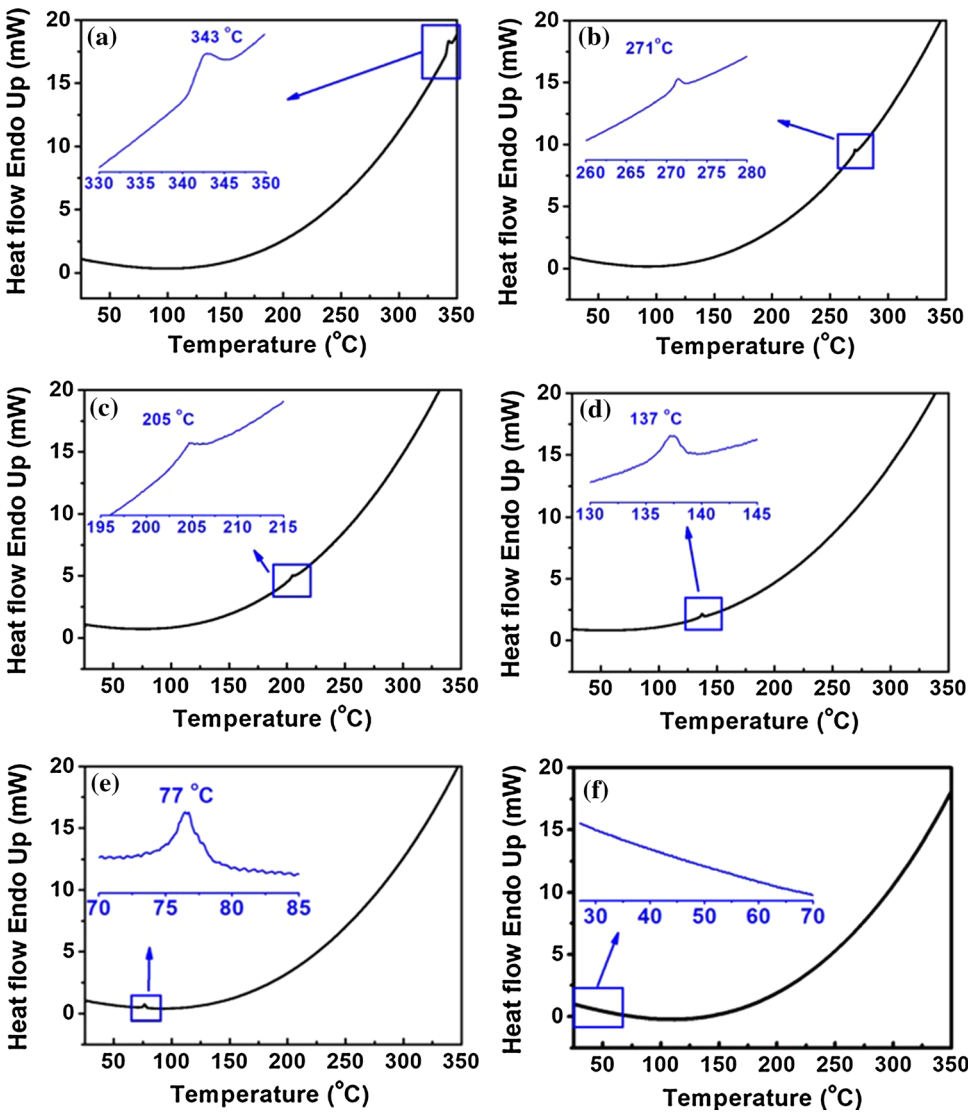

Figure 9 DSC curves of $In_{2-x}Sc_xMo_3O_{12}$ solid solutions **a** $In_2Mo_3O_{12}$, **b** $In_{1.7}Sc_{0.3}Mo_3O_{12}$, **c** $In_{1.4}Sc_{0.6}Mo_3O_{12}$, **d** $In_{1.1}Sc_{0.9}Mo_3O_{12}$, **e** $In_{0.8}Sc_{1.2}Mo_3O_{12}$ and **f** $In_{0.5}Sc_{1.5}Mo_3O_{12}$.

Theoretical calculation analysis

To analyze the structural stability of the $In_{2-x}Sc_xMo_3O_{12}$, the total energy of both monoclinic and orthorhombic phase $In_{2-x}Sc_xMo_3O_{12}$ is calculated by the framework of spin-polarized DFT as implemented in the Vienna Ab initio Simulation Package (VASP) [20, 21]. The exchange–correlation potentials were treated by the generalized gradient

Table 2 Phase transition temperature of obtained $In_{2-x}Sc_xMo_3O_{12}$ solid solutions using DSC and TMA

Samples	Phase transition temperature	
	DSC (°C)	TMA (°C)
$In_2Mo_3O_{12}$	343	334–355
$In_{1.7}Sc_{0.3}Mo_3O_{12}$	271	263–292
$In_{1.4}Sc_{0.6}Mo_3O_{12}$	205	200–216
$In_{1.1}Sc_{0.9}Mo_3O_{12}$	137	130–146
$In_{0.8}Sc_{1.2}Mo_3O_{12}$	77	75–85
$In_{0.5}Sc_{1.5}Mo_3O_{12}$	–	–

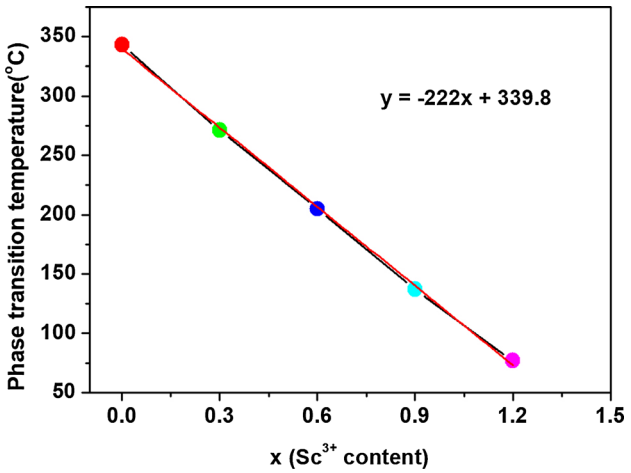

Figure 10 Phase transition temperature of $In_{2-x}Sc_xMo_3O_{12}$ solid solutions as a function of Sc^{3+}-content.

approximation (GGA) parameterized by Perdew, Burke and Ernzerhof (PBE) [22]. The interaction between valence electrons and ion cores was described by the projected augmented wave (PAW) method [23]. The monoclinic and orthorhombic phases of $In_{2-x}Sc_xMo_3O_{12}$ were modeled as a periodic slab by setting the lattice parameters as a = 16.34 Å/19.32 Å, b = 9.55 Å/13.23 Å and c = 18.76 Å/9.47 Å, respectively. The Monkhorst–Pack grid of 1 × 2 × 1 and 1 × 1 × 2 was used for the geometry optimization. A 400 eV kinetic energy cutoff was chosen for plane-wave basis set, and conjugated gradient (CG) atomic optimization was performed with a criterion of convergence of 0.01 eV/Å.

To address the phase transfer process of $In_{2-x}Sc_xMo_3O_{12}$, we compared the stabilities of the monoclinic and orthorhombic phase $In_{2-x}Sc_xMo_3O_{12}$ by displacing In atom with Sc atoms, at the ratios (R = Sc:In) of 0:6, 2:14, 4:12, 6:10, 8:8, 10:6, 12:4, 14:2 and 16:0, respectively (see Fig. 11a). Our results indicate that very close energies are found for these two phases at various doping ratios. This may be explained by the small difference in the two crystal structure. Normal XRD cannot tell the difference between monoclinic and orthorhombic phase of $In_2Mo_3O_{12}$ [4]. Only the XRD results obtained using a synchrotron facility can distinctly reveal the difference of the two structures. Figure 11b shows the energy difference (ΔE) between the monoclinic and orthorhombic phase $In_{2-x}Sc_xMo_3O_{12}$ with the same doping atomic ratio of Sc, and the ΔE is calculated as:

$$\Delta E = E_{\text{monoclinic}} - E_{\text{orthorhombic}}$$

A careful examination manifested that the energy profile of two phases crosses at around R = 12:4, which can be clearly seen in Fig. 11b. When R < 12:4,

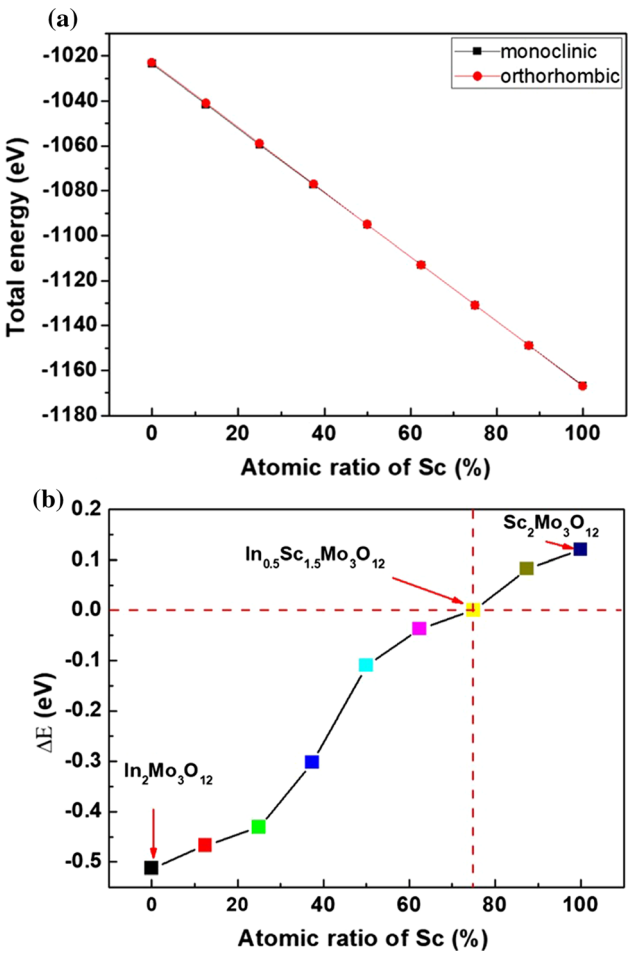

Figure 11 Calculated total energies (**a**) and energy difference (**b**) between monoclinic and orthorhombic phases of $In_{2-x}Sc_xMo_3O_{12}$ at various doping atomic ratios of Sc.

$\Delta E < 0$, indicating the $In_{2-x}Sc_xMo_3O_{12}$ has stable monoclinic phase, while an orthorhombic phase is energetically favored once $R \geq 12{:}4$. In other words, it means that the $In_{2-x}Sc_xMo_3O_{12}$ ($x < 1.5$) crystallizes in a monoclinic $In_2Mo_3O_{12}$-type symmetry, and when $x \geq 1.5$, the $In_{2-x}Sc_xMo_3O_{12}$ shows an orthorhombic $Sc_2Mo_3O_{12}$-type symmetry. These theoretical results accord well with our experimental evidences.

Conclusions

For the first time, single-phased $In_{2-x}Sc_xMo_3O_{12}$ solid solutions (x = 0, 0.3, 0.6, 0.9, 1.2 and 1.5) were synthesized by the chemical co-precipitation method. Sc^{3+}-substitution gave rise to a change in the crystal structure of $In_2Mo_3O_{12}$. $In_{2-x}Sc_xMo_3O_{12}$ adopts monoclinic $In_2Mo_3O_{12}$-type symmetry for $x \leq 1.2$ and transforms to orthorhombic $Sc_2Mo_3O_{12}$-type symmetry in the case of x = 1.5. Meanwhile, the co-precipitation synthesis leads to better densification and sinterability in the above samples. The microstructure of $In_{2-x}Sc_xMo_3O_{12}$ becomes denser with fine grain shape and narrow size distribution influenced by the increase in Sc^{3+}-content. Furthermore, Sc^{3+}-substitution at A-site of $In_2Mo_3O_{12}$ can effectively shift the phase transition temperature to below room temperature. The phase transition temperature of $In_{0.5}Sc_{1.5}Mo_3O_{12}$ is around 7 °C and shows stable negative thermal expansion. The corresponding average CTE of $In_{0.5}Sc_{1.5}Mo_3O_{12}$ ceramics is -5.08×10^{-6} °C^{-1} from 25 to 600 °C. The calculation results obtained using spin-polarized density functional theory agree well with the experimental results. When $R < 12{:}4$, the $In_{2-x}Sc_xMo_3O_{12}$ has stable monoclinic phase, while an orthorhombic phase is energetically favored once $R \geq 12{:}4$.

Acknowledgements

This work was supported by the National Natural Science Foundation of China [Grant Numbers 51602280, 51102207], Qing Lan Project of Jiangsu Province, University Natural Science Research Foundation of Jiangsu Province [Grant Number 14KJB430025] and Guangling College of Yangzhou University Natural Science Research Foundation [Grant Number ZKZD17001]. Thanks to Prof. Cora Lind for her suggestion and revision on the manuscript.

References

[1] Evans JSO, Mary TA, Sleight AW (1998) Negative thermal expansion in $Sc_2(WO_4)_3$. Solid State Chem 137:148–160

[2] Evans JSO, Mary TA (2000) Structural phase transitions and negative thermal expansion in $Sc_2Mo_3O_{12}$. Int J Inorg Mater 2:143–151

[3] Evans JSO, Mary TA, Sleight AW (1997) Negative thermal expansion in a large molybdate and tungstate family. Solid State Chem 133:580–583

[4] Marinkovic BA, Ari M, Jardim PM et al (2010) $In_2Mo_3O_{12}$: a low negative thermal expansion compound. Thermochim Acta 499:48–53

[5] Liu HF, Zhang ZP, Ma J et al (2015) Effect of isovalent substitution on phase transition and negative thermal expansion of $In_{2-x}Sc_xW_3O_{12}$ ceramics. Ceram Int 41:9873–9877

[6] Sumithra S, Umarji AM (2004) Role of crystal structure on the thermal expansion of $Ln_2W_3O_{12}$ (Ln = La, Nd, Dy, Y, Er and Yb). Solid State Sci 6:1313–1319

[7] Xiao XL, Wu MM, Peng J et al (2008) Negative thermal expansion of $Yb_2Mo_3O_{12}$ and $Lu_2Mo_3O_{12}$[C]. Key Eng Mater 368:1662–1664

[8] Sumithra S, Tyagi AK, Umarji AM (2005) Negative thermal expansion in $Er_2W_3O_{12}$ and $Yb_2W_3O_{12}$ by high temperature X-ray diffraction. Mater Sci Eng B 116:14–18

[9] Xiao XL, Cheng YZ, Peng J et al (2008) Thermal expansion properties of $A_2(MO_4)_3$ (A = Ho and Tm; M = W and Mo). Solid State Sci 10:321–325

[10] Forster PM, Yokochi A, Sleight AW (1998) Enhanced negative thermal expansion in $Lu_2W_3O_{12}$. Solid State Chem 140:157–158

[11] Liu HF, Zhang W, Zhang ZP et al (2009) Synthesis and negative thermal expansion properties of solid solutions $Yb_{2-x}La_xW_3O_{12}$ ($0 \leq x \leq 2$). Ceram Int 35:2951–2956

[12] Cheng YZ, Xiao XL, Liu XF et al (2013) Study of the structures and thermal expansion properties of solid solutions $Yb_{2-x}Dy_xW3O12$ ($0 \leq x \leq 1.5$ and $1.8 \leq x \leq 2.0$). Phys B Condens Matter 411:173–177

[13] Cheng YZ, Wu MM, Peng J et al (2007) Structures, thermal expansion properties and phase transitions of $Er_xFe_{2-x}Mo_3O_{12}$ ($0.0 \leq x \leq 2.0$). Solid State Sci 9:693–698

[14] Wu MM, Peng J, Cheng YZ et al (2007) Thermal expansion in solid solution $Er_{2-x}Sm_xW_3O_{12}$. Mater Sci Eng B 137:144–148

[15] Vinet P, Rose JH, Ferrante J et al (1989) Universal features of the equation of state of solids. J Phys Condens Matter 1:1941–1963

[16] Wu MM, Peng J, Yong Z et al (2012) Thermal expansion properties of Lu_{2-x} $Fe_xMo_3O_{12}$. Chin Phys B 21:346–351

[17] Tyagi AK, Achary SN, Mathews MD (2002) Phase transition and negative thermal expansion in $A_2Mo_3O_{12}$ system (A = Fe^{3+}, Cr^{3+} and Al^{3+}). J Alloy Compd 339:207–210

[18] Zhang ZP, Yang L, Zhu Q et al (2017) Phase transition and negative thermal expansion properties in isovalently substituted $In_{2-x}Sc_xMo_3O_{12}$ ceramics. Ceram Int 43:12013–12017

[19] Maczka M, Hermanowicz K, Hanuza J (2005) Phase transition and vibrational properties of $A_2(BO_4)_3$ compounds (A = Sc, In; B = Mo, W). J Mol Struct 744:283–288

[20] Kresse G, Hafner J (1993) Ab initio molecular dynamics for open-shell transition metals. Phys Rev B 48:13115–13118

[21] Kresse G, Furthmüller J (1996) Efficiency of ab initio total energy calculations for metals and semiconductors using a plane-wave basis set. Comput Mater Sci 6:15–50

[22] Perdew JP, Burke K, Ernzerhof M (1996) Generalized gradient approximation made simple. Phys Rev Lett 77:3865–3868

[23] Blochl PE (1994) Projector augmented-wave method. Phys Rev B 50:17953–17979